Inorg. Chem. **2008**, *47*, 6829−6839

Oxalate-Based Soluble 2D Magnets: The Series $[K(18\text{-crown-6})]_3[M^{II}_3(H_2O)_4\{M^{III}(ox)_3\}_3]$ (M^{III} = Cr, Fe; M^{II} = Mn, Fe, Ni, Co, Cu; ox = $C_2O_4^{2-}$; 18-crown-6 = $C_{12}H_{24}O_6$)

Eugenio Coronado,*,† José R. Galán-Mascarós,*,† Carlos Martí-Gastaldo,† João C. Waerenborgh,‡ and Piotr Gaczyński‡

Instituto de Ciencia Molecular, Universidad de Valencia, Polígono de la Coma s/n, 46980, Paterna (Spain), and Inst. Tecnológico e Nuclear, CFMC-UL, Department of Chemistry, Estrada Nacional 10, 2686-953 Sacavém (Portugal)

Received March 7, 2008

The synthesis and magnetic properties of the oxalate-based molecular soluble magnets with general formula $[K(18\text{-crown-6})]_3[M^{II}_3(H_2O)_4\{M^{III}(ox)_3\}_3]$ (M^{III} = Cr, Fe; M^{II} = Mn, Fe, Ni, Co, Cu; ox = $C_2O_4^{2-}$) are here described. All the reported compounds are isostructural and built up by 2D bimetallic networks formed by alternating M^{III} and M^{II} ions connected through oxalate anions. Whereas the $Cr^{III}M^{II}$ derivatives behave as ferromagnets with critical temperatures up to 8 K, the $Fe^{III}M^{II}$ present ferri- or weak ferromagnetic ordering up to 26 K.

Introduction

In the last decades, important attention has been devoted to molecular magnetism, producing a large number of molecule-based magnets. These materials appear as promising candidates to emulate classical inorganic solids[1] as they combine physical properties, such as electrical conductivity or ferromagnetism, which have been always associated with classic solid-state materials, with their intrinsic properties: biocompatibility, easy processability, or lightness. The physical properties of these materials are mainly defined by their topology and the chemical nature of the constituents. With this in mind, a suitable choice of the molecular building-blocks can lead to remarkable control on the resulting materials properties.

Among these oxalate-based magnets, those presenting a layered structure are remarkable. Its layered topology introduces versatile chemistry, as the change of the molecular component within the layers, attending to its size, geometry, or electronic structure, can easily tune the magnetic properties in the final compound. The bis-chelating coordination ability of the oxalate ion and its capacity to promote magnetic interaction between paramagnetic centers has made it a useful and versatile choice in the design of many different magnetic architectures. The first example in this direction dates from the early 90s when the family of compounds: $[A][M^{II}M^{II}(ox)_3]$ ($A = NR_4^+$, PPh_4^+; M^{II} = Mn, Fe, Co, Ni, Cu, Zn; M^{III} = Cr, Fe) was reported by Okawa et al. These compounds behave as ferro-,[2] ferri-,[3–5] or canted antiferromagnets[6,7] with critical temperatures in the 5 to 43 K threshold. These bimetallic salts[8] are composed by a polymeric 2D honeycomb-like anionic network with general formula $[M^{II}M^{III}(ox)_3]^-$ and a bulky alkylammonium cation $[A]^+$. This cation acts as a templating agent, thus controlling the network formation and determining its packing as well as the interlayer separation. To increase the complexity of these systems, the electronically innocent cation can be substituted by an electroactive one with the objective of conferring a novel property to the final material; this strategy

* To whom correspondence should be addressed. E-mail: eugenio.coronado@uv.es jose.r.galan@uv.es. Phone: +34-963544415. Fax: +34-963543273.
† Universidad de Valencia.
‡ Inst. Tecnológico e Nuclear.

(1) Miller, J. S. *Adv. Mater.* **1990**, *2*, 378–379.
(2) Tamaki, H.; Zhong, Z. J.; Matsumoto, N.; Kida, S.; Koikawa, M.; Achiwa, N.; Hashimoto, Y.; Okawa, H. *J. Am. Chem. Soc.* **1992**, *114*, 6974–6979.
(3) Larionova, J.; Mombelli, B.; Sanchiz, J.; Kahn, O. *Inorg. Chem.* **1998**, *37*, 679–684.
(4) Okawa, H.; Matsumoto, N.; Tamaki, H.; Ohba, M. *Mol. Cryst. Liq. Cryst.* **1993**, *232*, 617–622.
(5) Tamaki, H.; Mitsumi, M.; Nakamura, K.; Matsumoto, N.; Kida, S.; Okawa, H.; Iijima, S. *Chem. Lett.* **1992**, 1975–1978.
(6) Mathoniere, C.; Nuttall, C. J.; Carling, S. G.; Day, P. *Inorg. Chem.* **1996**, *35*, 1201–1206.
(7) Mathoniere, C.; Carling, S. G.; Dou, Y. S.; Day, P. *J. Chem. Soc., Chem. Commun.* **1994**, 1551–1552.
(8) Decurtins, S.; Schmalle, H. W.; Oswald, H. R.; Linden, A.; Ensling, J.; Gutlich, P.; Hauser, A. *Inorg. Chim. Acta* **1994**, *216*, 65–73.

10.1021/ic800418k CCC: $40.75 © 2008 American Chemical Society
Published on Web 07/01/2008

Table 1. Refined Unit Cell Constants of $[K(18\text{-crown-}6)]_3[M^{II}_3(H_2O)_4\{M^{III}(ox)_3\}_3]$ (M^{III} = Cr, Fe; M^{II} = Mn, Fe, Ni, Co, Cu; ox = $C_2O_4^{2-}$)

$M^{III}M^{II}$	a [Å]	b [Å]	c [Å]	β [degrees]	V [Å^3]
CrMn[a]	26.776(6)	20.049 (5)	18.190 (5)	115.93(4)	8781(4)
CrMn	26.61(6)	19.57(5)	18.27(3)	114.6(3)	8653(2)
CrFe	26.65(8)	19.81(7)	18.11(5)	115.5(4)	8632(3)
CrCo	26.79(1)	20.54(1)	18.10(4)	117.9(4)	8806(5)
CrNi	26.35(2)	20.78(7)	17.91(3)	117.1(6)	8735(3)
CrCu	26.28(7)	19.27(6)	18.15(3)	113.6(2)	8419(3)
FeMn	26.91(5)	20.50(5)	18.27(6)	116.8(7)	8984(3)
FeFe	26.40(6)	19.89(6)	18.10(9)	115.3(5)	8583(3)
FeCo	26.26(1)	21.32(6)	17.98(8)	119.1(3)	8797(8)
FeNi	26.22(9)	19.81(5)	18.03(6)	114.5(6)	8525(3)

[a] Cell constants obtained from single-crystal X-ray diffraction measurements.

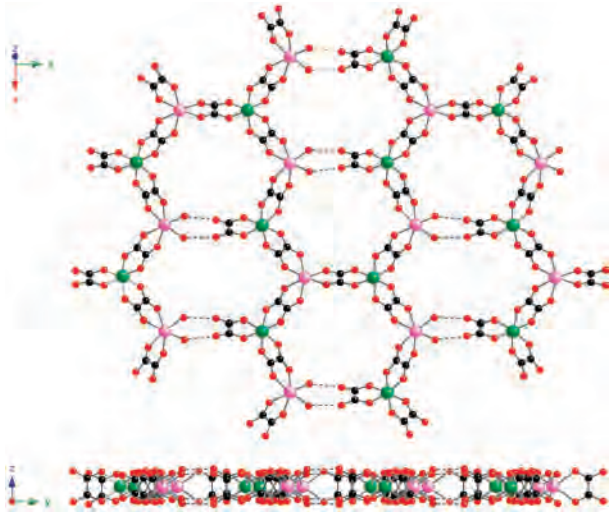

Figure 1. Perspective showing the pseudohexagonal configuration of the 2D fragmented anionic polymeric network (up). View of the layered nature of the oxalate-based compound in the solid state (down).

has successfully led to the preparation of magnetic multilayers,[9] ferromagnetic molecular metals,[10] or photo chromic magnets.[11,12]

The oxalate ligand's ability to generate many different structural topologies by controlling the synthetical process has been widely demonstrated. In fact, the use of a capping ligand results in a reduction of the dimensionality of the bimetallic oxalate-based complexes formed. Following this synthetically strategy several oligomeric species such as dimers,[13–16] trimers,[17,18] and tetramers[19,20] have been successfully obtained. On the other hand, selecting the appropriated templating counter-ions can increase the dimensionality of these oxalate-based systems. This strategy led in the past to the preparation of the 3D families $[Z(bpy)_3]^{21}[MM'(ox)_3]^{22–25}$ and $[Z'(ppy)(bpy)_2][MM'(ox)_3]^{26,27}$ (Z = Fe^{II}, Co^{II}, Ni^{II}, and Ru^{II}; Z′ = Ru^{I}, Ir^{I}; X = ClO_4^-, BF_4^-, and PF_6^-; M, M′ = Li^{I}, Na^{I}, Mn^{II}, Ni^{II}, Co^{II}, Fe^{II}, Cu^{II}, Zn^{II}, Rh^{III}, Co^{III}, Cr^{III}, and Fe^{III}; bpy = 2,2′-dipyridyl, ppy = phenylpyridine). In these cases, the tris-bipyridyl chiral complexes, presenting the appropriate D_3 symmetry, force the $[M^{III}(ox)_3]^{3-}$ building blocks to adopt a homochiral configuration (ΔΔ or ΛΛ). Therefore, these polymers cannot adopt a planar disposition (analogous to a 2D network), and it is not possible for the system to stay in the plane with only one diastereoisomeric building block, but they give raise to 3D extended networks. These higher dimensional systems present ferri- and ferromagnetic behavior but with lower critical temperatures than their 2D analogous. The longer metal−metal distances and the different magnetic orbitals relative orientation in the 3D framework imposed by the metallic homochiral configuration, thus resulting in a weaker magnetic exchange, could possibly explain this point.

Considering the strong influence of the templating counterion in the stabilization and isolation of these systems, we considered $[K\text{-}18\text{-crown-}6]^+$ a promising candidate, as its size, charge, and geometry could result in the obtention of new magnetically interesting oxalate-based architectures. Now, we have extended this strategy to successfully control the dimensionality of oxalate-based bimetallic complexes, from 1D chains[28,29] to 2D phases.[30] Here, we report on the synthesis and physical characterization of the 2D family: $[K(18\text{-crown-}6)]_3[M^{II}_3(H_2O)_4\{M^{III}(ox)_3\}_3]$ (M^{III} = Cr, Fe; M^{II} = Mn, Fe, Ni, Co, Cu; ox = $C_2O_4^{2-}$).

Experimental Section

Synthesis. All reagents and solvents used were of commercially available grade and were used without any previous purification. $K_3[M^{III}(ox)_3]$ (M^{III} = Cr, Fe) complexes were prepared according

(9) Coronado, E.; Galan-Mascaros, J. R.; Gomez-Garcia, C. J.; Ensling, J.; Gutlich, P. *Chem.—Eur. J.* **2000**, *6*, 552–563.
(10) Coronado, E.; Galan-Mascaros, J. R.; Gomez-Garcia, C. J.; Laukhin, V. *Nature* **2000**, *408*, 447–449.
(11) Benard, S.; Yu, P.; Audiere, J. P.; Riviere, E.; Clement, R.; Guilhem, J.; Tchertanov, L.; Nakatani, K. *J. Am. Chem. Soc.* **2000**, *122*, 9444–9454.
(12) Benard, S.; Riviere, E.; Yu, P.; Nakatani, K.; Delouis, J. F. *Chem. Mater.* **2001**, *13*, 159–162.
(13) Roman, P.; GuzmanMiralles, C.; Luque, A.; Beitia, J. I.; Cano, J.; Lloret, F.; Julve, M.; Alvarez, S. *Inorg. Chem.* **1996**, *35*, 3741–3751.
(14) Triki, S.; Berezovsky, F.; Pala, J. S.; Coronado, E.; Gomez-Garcia, C. J.; Clemente, J. M.; Riou, A.; Molinie, P. *Inorg. Chem.* **2000**, *39*, 3771–3776.
(15) Kahn, O. *Angew. Chem., Int. Ed.* **1985**, *24*, 834–850.
(16) Coronado, E.; Galan-Mascaros, J. R.; Gomez-Garcia, C. J. *J. Chem. Soc., Dalton Trans.* **2000**, 205–210.
(17) Rochon, F. D.; Melanson, R.; Andruh, M. *Inorg. Chem.* **1996**, *35*, 6086–6092.
(18) Andruh, M.; Melanson, R.; Stager, C. V.; Rochon, F. D. *Inorg. Chim. Acta* **1996**, *251*, 309–317.
(19) Marinescu, G.; Andruh, M.; Lescouezec, R.; Munoz, M. C.; Cano, J.; Lloret, F.; Julve, M. *New J. Chem.* **2000**, *24*, 527–536.
(20) Coronado, E.; Gimenez, M. C.; Gomez-Garcia, C. J.; Romero, F. M. *Polyhedron* **2003**, *22*, 3115–3122.
(21) Pellaux, R.; Schmalle, H. W.; Huber, R.; Fischer, P.; Hauss, T.; Ouladdiaf, B.; Decurtins, S. *Inorg. Chem.* **1997**, *36*, 2301–2308.
(22) Coronado, E.; Galan-Mascaros, J. R.; Gomez-Garcia, C. J.; Martinez-Agudo, J. M. *Inorg. Chem.* **2001**, *40*, 113–120.
(23) Hernandez-Molina, M.; Lloret, F.; Ruiz-Perez, C.; Julve, M. *Inorg. Chem.* **1998**, *37*, 4131–4135.
(24) Decurtins, S.; Schmalle, H. W.; Schneuwly, P.; Ensling, J.; Gutlich, P. *J. Am. Chem. Soc.* **1994**, *116*, 9521–9528.
(25) Decurtins, S.; Schmalle, H. W.; Schneuwly, P.; Oswald, H. R. *Inorg. Chem.* **1993**, *32*, 1888–1892.
(26) Clemente-Leon, M.; Coronado, E.; Gomez-Garcia, C. J.; Soriano-Portillo, A. *Inorg. Chem.* **2006**, *45*, 5653–5660.
(27) Pointillart, F.; Train, C.; Gruselle, M.; Villain, F.; Schmalle, H. W.; Talbot, D.; Gredin, P.; Decurtins, S.; Verdaguer, M. *Chem. Mater.* **2004**, *16*, 832–841.
(28) Coronado, E.; Galan-Mascaros, J. R.; Gomez-Garcia, C. J.; Marti-Gastaldo, C. *Inorg. Chem.* **2005**, *44*, 6197–6202.
(29) Coronado, E.; Galan Mascaros, J. R.; Marti-Gastaldo, C. *Polyhedron* **2007**, *26*, 2101–2104.
(30) Coronado, E.; Galan-Mascaros, J. R.; Marti-Gastaldo, C. *Inorg. Chem.* **2006**, *45*, 1882–1884.

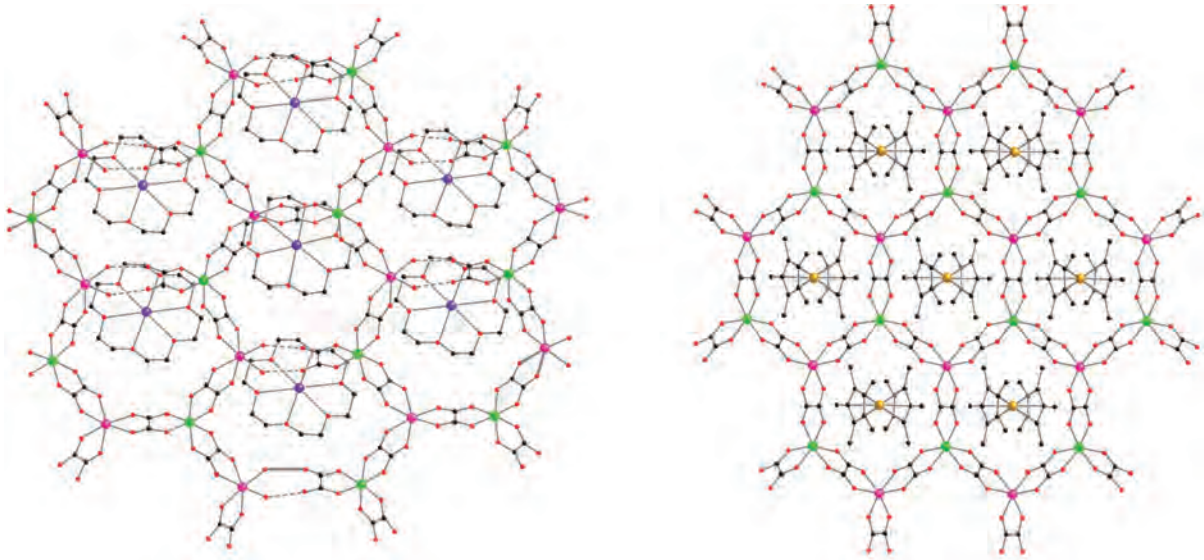

Figure 2. Perspective showing the relative orientation of the cationic complexes ($[K(18\text{-crown-6})]^+$and $[FeCp^*_2]^+$) with respect to the oxalate-based 2D framework for **1** (left) and $[FeCp^*_2][MnCr(ox)_3]$ (right).

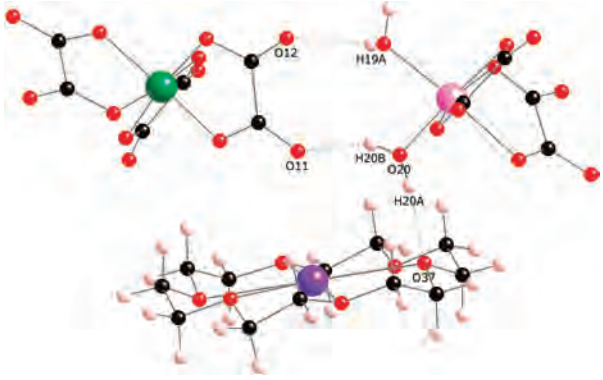

Figure 3. Picture depicting the hydrogen-bonding interactions along the anionic network and between the crown ether cationic complex and the coordinating water molecules belonging to the oxalate-based framework.

to previously described methods. All reactions were carried under laboratory atmosphere apart from those concerning iron(II) that were carried under argon atmosphere to avoid the precursor oxidation. The precursor $K_3[Fe(ox)_3]$ is light sensitive, attending to this point, all of the iron(III) derivatives were synthesized in absence of light to avoid the presence of iron(II) impurities in the final compounds.

$[K(18\text{-crown-6})]_3[Mn_3(H_2O)_4\{Cr(ox)_3\}_3]$ (**1**): $K_3[Cr(ox)_3]\cdot 3H_2O$ (1 mmol, 0.487 g) and 18-crown-6 ether (5 mmol, 1.32 g) were dissolved in 15 mL of methanol, giving rise to a dark-violet solution, $MnCl_2\cdot 4H_2O$ (1 mmol, 0.197 g) dissolved in 5 mL of methanol was added dropwise, immediately a purple precipitate appeared, and the mixture was stirred for 15 min. The methanolic solution is filtered in vacuo, the precipitate is washed with methanol and dried to vacuum. Yield: 65%. Anal. Calcd for C_{54} O_{58} H_{80} $K_3Mn_3Cr_3$ (2095.29): C, 30.95; H, 3.85. Found: C, 30.97; H, 3.85. Single crystals suitable for X-ray diffraction were prepared by slow diffusion of a methanolic solution (15 mL) of [K-(18-crown-6)$_3$]-$[Cr(ox)_3]$ (0.751 g, 1 mmol) into an aqueous solution (10 mL) of $MnCl_2\cdot 4H_2O$ (0.198 g, 1 mmol). After 24 h, purple rhombohedral crystals grown in the interphase were collected by hand, washed thoroughly with methanol, and dried in air.

(31) Thetiot, F.; Triki, S.; Pala, J. S.; Gomez-Garcia, C. J.; Golhen, S. *Chem. Commun.* **2002**, 1078–1079.

$[K(18\text{-crown-6})]_3[Fe_3(H_2O)_4\{Cr(ox)_3\}_3]$ (**2**): is obtained following the same procedure described above for **1** but using $FeCl_2\cdot 4H_2O$ (1 mmol, 0.199 g) instead of $MnCl_2\cdot 4H_2O$. **2** is isolated as a yellow precipitate. Yield: 68%. Anal. Calcd for C_{54} O_{58} H_{80} $K_3Fe_3Cr_3$ (2098.01): C, 30.91; H, 3.84. Found: C, 30.68; H, 3.85.

$[K(18\text{-crown-6})]_3[Co_3(H_2O)_4\{Cr(ox)_3\}_3]$ (**3**): is obtained using $CoCl_2\cdot 6H_2O$ (1 mmol, 0.238 g) and isolated as a purple precipitate. Yield: 59%. Anal. Calcd for C_{54} O_{58} H_{80} $K_3Co_3Cr_3$ (2107.27): C, 30.78; H, 3.83. Found: C, 30.57; H, 3.81.

$[K(18\text{-crown-6})]_3[Ni_3(H_2O)_4\{Cr(ox)_3\}_3]$ (**4**): is obtained using $NiCl_2\cdot 6H_2O$ (1 mmol, 0.238 g) and isolated as a green precipitate. Yield: 62%. Anal. Calcd for C_{54} O_{58} H_{80} $K_3Ni_3Cr_3$ (2106.56): C, 30.79; H, 3.83. Found: C, 30.82; H, 3.69.

$[K(18\text{-crown-6})]_3[Cu_3(H_2O)_4\{Cr(ox)_3\}_3]$ (**5**): is obtained using $CuCl_2\cdot 2H_2O$ (1 mmol, 0.170 g) and isolated as a blue precipitate. Yield: 53%. Anal. Calcd for C_{54} O_{58} H_{80} $K_3Cu_3Cr_3$ (2121.11): C, 30.58; H, 3.80. Found: C, 30.60; H, 3.79.

$[K(18\text{-crown-6})]_3[Mn_3(H_2O)_4\{Fe(ox)_3\}_3]$ (**6**): $Fe_3[Cr(ox)_3]\cdot 3H_2O$ (1 mmol, 0.491 g) and 18-crown-6 ether (5 mmol, 1.32 g) were dissolved in 15 mL of methanol giving rise to a green solution, $MnCl_2\cdot 4H_2O$ (1 mmol, 0.197 g) dissolved in 5 mL of methanol was added dropwise, inmediatly a yellow precipitate appeared, and the mixture was stirred for 15 min. The methanolic solution is filtered in vacuo, the precipitate is washed with methanol and dried to vacuum. Yield: 72%. Anal. Calcd for C_{54} O_{58} H_{80} $K_3Mn_3Fe_3$ (2106.83): C, 30.79; H, 3.83. Found: C, 30.74; H, 3.80.

$[K(18\text{-crown-6})]_3[Fe_3(H_2O)_4\{Fe(ox)_3\}_3]$ (**7**): is obtained following the same procedure described above for **6** but using $FeCl_2\cdot 4H_2O$ (1 mmol, 0.199 g) instead of $MnCl_2\cdot 4H_2O$. **7** is isolated as a yellow precipitate. Yield: 70%. Anal. Calcd for C_{54} O_{58} H_{80} $K_3Fe_3Fe_3$ (2109.56): C, 30.75; H, 3.82. Found: C, 30.25; H, 3.78.

$[K(18\text{-crown-6})]_3[Co_3(H_2O)_4\{Fe(ox)_3\}_3]$ (**8**): is obtained by using $CoCl_2\cdot 6H_2O$ (1 mmol, 0.238 g) and isolated as a yellow precipitate. Yield: 69%. Anal. Calcd for C_{54} O_{58} H_{80} $K_3Co_3Fe_3$ (2118.82): C, 30.61; H, 3.81. Found: C, 30.07; H, 3.86.

$[K(18\text{-crown-6})]_3[Ni_3(H_2O)_4\{Fe(ox)_3\}_3]$ (**9**): is obtained by using $NiCl_2\cdot 6H_2O$ (1 mmol, 0.238 g) and isolated as a yellow precipitate. Yield: 68%. Anal. Calcd for C_{54} O_{58} H_{80} $K_3Ni_3Fe_3$ (2118.10): C, 30.62; H, 3.81. Found: C, 29.82; H, 3.90.

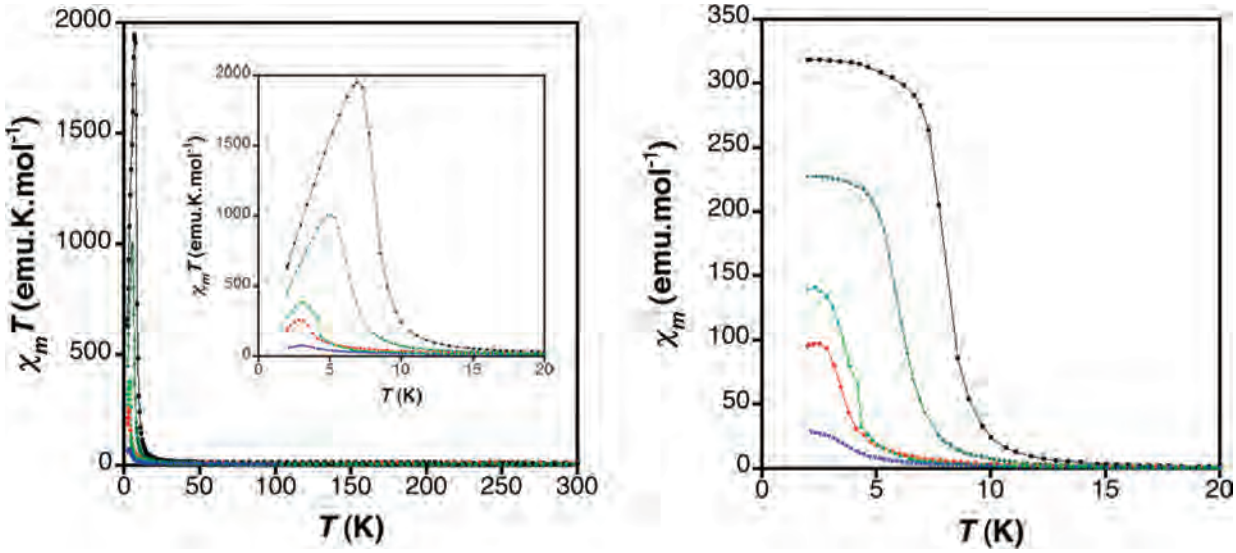

Figure 4. Plot of $\chi_M T$ product vs T for $[K(18\text{-crown-}6)]_3[M^{II}_3(H_2O)_4\{Cr(ox)_3\}_3]$ compounds. Inset corresponds to the low-temperature regime (left). Plot of the χ_M temperature dependence below 20 K (right). M^{II} = Mn (•), Fe (■), Co (◆), Ni (▲), and Cu (▼).

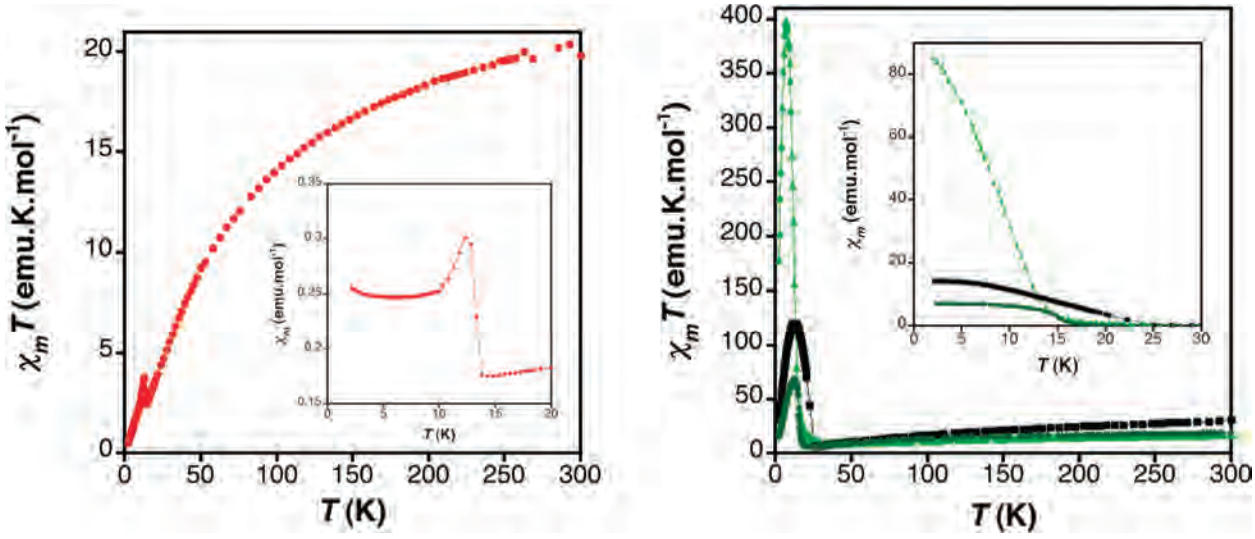

Figure 5. Plot of $\chi_M T$ product vs T for **6** (left) and **7**−**9** (right) compounds. Inset corresponds to χ_M temperature dependence in the low-temperature regime. M^{II} = Mn (•), Fe (■), Co (◆), and Ni (▲).

Physical Characterization.

X-ray data collection and analysis. A purple rhombohedral crystal of **1** was collected by hand and was mounted on a Nonius-Kappa CCD single cristal diffractometer using graphite-monochromated Mo Kα radiation (λ = 0.71073 Å) at 293 K. Data collection was performed by using the program *Collect*.[45] Data reduction and cell refinement were performed with the programs *Denzo* and *Scalepack*.[46] Crystal structure was solved by direct methods using the program *SIR97*,[47] followed by Fourier synthesis and refined on F^2 with *SHELXL-97*.[48] Anisotropic least-squares refinement of non-hydrogen atoms was performed. Hydrogen atoms positions were located geometrically. CCDC 280068 contains the supplementary crystallographic data for this paper. It can be obtained free of charge via www.ccdc.cam.ac.uk/retrieving.html or from Cambridge Crystallographic Data Center (12 Union Road, Cambridge CB2 1EZ, U.K., fax: (+44) 1223−336−033, deposit@ccdc.cam.ac.uk). All crystallographic plots were obtained via the *CrystalMaker* program.[49] X-ray powder profiles were collected with a Siemens d-500 X-ray diffractometer (Cu Kα radiation, λ_α = 1.54184 Å) at 293(2) K. Samples were grounded and mounted on a flat sample plate. Typically, profiles were collected as step scans over a 12 h period in the 2° < 2Θ < 60° range with a step size of 0.02°. Theoretical X-ray diffraction pattern for compound **1** was simulated from the atomic coordinates of its crystalline structure[30] using the *CrystalDiffract* software package.[50] X-ray diffraction data for **2**−**9** were indexed on a monoclinic space group and refined using the *Unitcell* program.[51]

(32) Bellouard, F.; Clemente-Leon, M.; Coronado, E.; Galan-Mascaros, J. R.; Gomez-Garcia, C. J.; Romero, F.; Dunbar, K. R. *Eur. J. Inorg. Chem.* **2002**, 1603–1606.
(33) Iijima, S.; Katsura, T.; Tamaki, H.; Mitsumi, M.; Matsumoto, N.; Okawa, H. *Mol. Cryst. Liq. Cryst.* **1993**, *232*, 623–628.
(34) Bhattacharjee, A.; Iijima, S.; Mizutani, F. *J. Magn. Magn. Mater.* **1996**, *153*, 235–240.
(35) Iijima, S.; Mizutani, F. *Mol. Cryst. Liq. Cryst. Sci. Technol., Sect. A* **1997**, *306*, 227–234.
(36) Ruebenbauer, K.; Birchall, T. *Hyperfine Interact.* **1979**, *7*, 125–133.
(37) Atovmyan, L. O.; Shilov, G. V.; Ovanesyan, N. S.; Pyalling, A. A.; Lyubovskaya, R. N.; Zhilyaeva, E. I.; Morozov, Y. G. *Synth. Met.* **1995**, *71*, 1809–1810.
(38) Coronado, E.; Galan-Mascaros, J. R.; Gomez-Garcia, C. J.; Martinez-Agudo, J. M.; Martinez-Ferrero, E.; Waerenborgh, J. C.; Almeida, M. *J. Solid State Chem.* **2001**, *159*, 391–402.

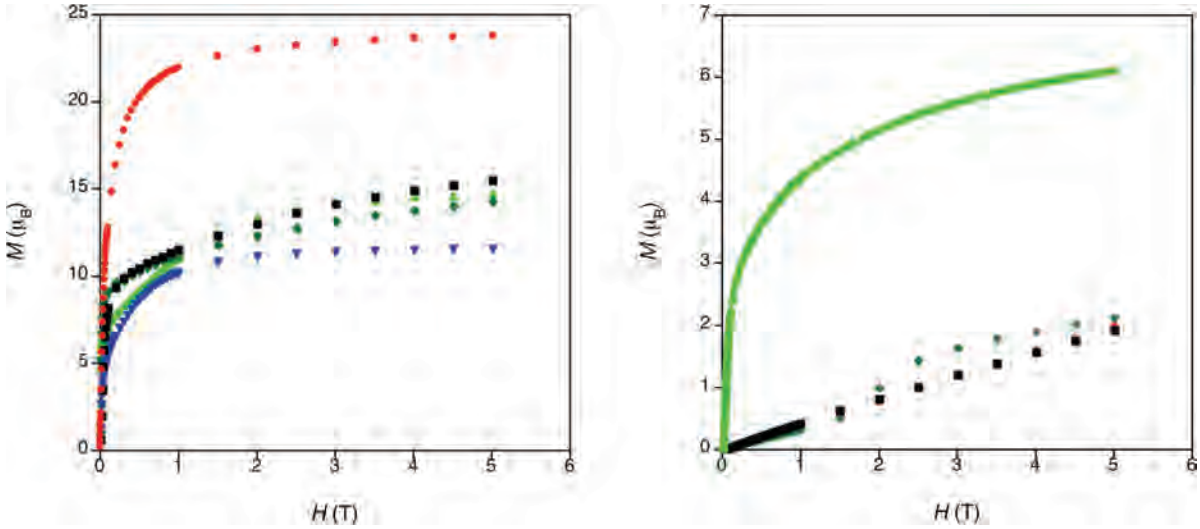

Figure 6. Field dependence of the magnetization at 2 K for **1**−**5** (left) and **6**−**9** (right).

Table 2. Hydrogen-Bond Parameters (Angstroms, Degrees)

	D−H	H···A	D···A	D−H···A
O19−H19A···O12	0.843(8)	2.086(1)	2.634(1)	122.16(8)
O20−H20B···O11	0.797(6)	1.846(6)	2.587(5)	154.08(2)
O20−H20A···O37	0.811(0)	1.930(4)	2.738(1)	173.86(4)

Elemental analysis. Carbon, nitrogen, and hydrogen contents were determined by microanalytical procedures using an EA 1110 CHNS-O Elemental Analyzer from CE Instruments.

Metallic Microanalysis. Metallic composition of bulk samples was determined by electron probe microanalysis (EPMA) performed in a Philips SEM XL30 equipped with an EDAX DX-4 microsonde.

FTIR. Infrared spectra were recorded in an FTIR Nicolet 5700 sprectometer in the 4000−400 cm^{-1} range using powdered samples in KBr pellets.

Magnetic characterization. Magnetic susceptibility measurements were performed on polycrystalline samples with a Quantum Design MPMS-XL-5 susceptometer equipped with a SQUID sensor. The susceptibility data were corrected from the diamagnetic contributions as deduced by using Pascal's constant tables. dc data were collected in the range 2−300 K with an applied field of 100 and 1000 G, and hysteresis loops were collected between −5 and +5 T at 2 K. ac data were collected in the range 2−30 K with an applied alternating field of 3.95 G at different frequencies in the range 1−1000 Hz.

Mössbauer spectroscopy. Mössbauer spectra were collected in transmission mode using a conventional constant-acceleration spectrometer and a 25 mCi ^{57}Co source in a rhodium matrix. The velocity scale was calibrated using α-Fe foil. The absorbers were obtained by pressing the powdered samples into perspex holders. Isomer shifts (*IS*) are given relative to metallic α-Fe at room temperature. Low-temperature spectra were collected using either a liquid-helium flow cryostat with a temperature stability of ± 0.5 K or a bath cryostat, model SVT-400, with the sample immersed in liquid helium, for measurements at or below 4.1 K. The spectra were fitted to Lorentzian lines using a nonlinear least-squares method.[52]

(39) Carling, S. G.; Visser, D.; Hautot, D.; Watts, I. D.; Day, P.; Ensling, J.; Gutlich, P.; Long, G. J.; Grandjean, F. *Phys. Rev. B: Condens. Matter* **2002**, *66*, 104407.

Results and Discussion

Synthesis and Structure. We have synthesized a total of nine compounds divided into two different series namely: the chromium(III) series $[K(18\text{-crown-}6)]_3[M^{II}_3(H_2O)_4\{Cr(ox)_3\}_3]$ (M^{II} = Mn, Fe, Co, Ni, Cu) **1**−**5** and the iron(III) series $[K(18\text{-crown-}6)]_3[M^{II}_3(H_2O)_4\{Fe(ox)_3\}_3]$ (M^{II} = Mn, Fe, Co, Ni) **6**−**9**. All of the compounds have been isolated following the same synthetic route: dropwise addition of a M^{II} metallic salt methanolic solution to the corresponding $[K(18\text{-crown-}6)]_3[M^{III}(ox)_3]$ complex dissolved in methanol. We attempted to obtain the copper(II)−iron(III) derivative by slightly modifying the preparative route, but it was not possible to obtain a pure enough compound. This point is not surprising in view of the previous attempts in this sort of 2D bimetallic phases that never led to success when using copper(II) and iron(III) as the metallic constituents of the network. All of the compounds were obtained as polycrystalline powders as a result of the synthetic procedure and were structurally characterized by powder X-ray diffraction. The powder diffraction profiles show that all compounds are isostructural and exhibit analogous diffraction patterns to that simulated from the atomic positional parameters of the previously reported $[K(18\text{-crown-}6)]_3[Mn_3(H_2O)_4\{Cr(ox)_3\}_3]$,[30] which crystallizes in the *C*2/*c* monoclinic space group (Supporting Information). The crystallinity of **1**−**9** is high enough to allow for the reflections indexation, and unit-cell constants were refined on a monoclinic cell. The values of cell constants obtained are summarized in Table 1. Single crystals of **1** were obtained by slow diffusion of a methanolic solution of the $[K(18\text{-crown-}6)]_3[Cr(ox)_3]$ complex into an aqueous solution of $MnCl_2$. These salts crystallize in the *C*2/*c* monoclinic space group and are composed by alternating cationic and anionic layers. The stoichiometry of the latter corresponds to the formula $\{M^{II}_3(H_2O)_4[M^{III}(ox)_3]_3\}^{3-}$, and it is a polymeric oxalate-based network reminiscent of the well-known hexagonal honeycomb $[M^{II}M^{III}(ox)_3]^-$ structure (Figure 1). The most remarkable difference of this novel structure if compared to the classical 2D oxalate-based system is the presence of coordinating water molecules in some of the M^{II} ions conforming the network.

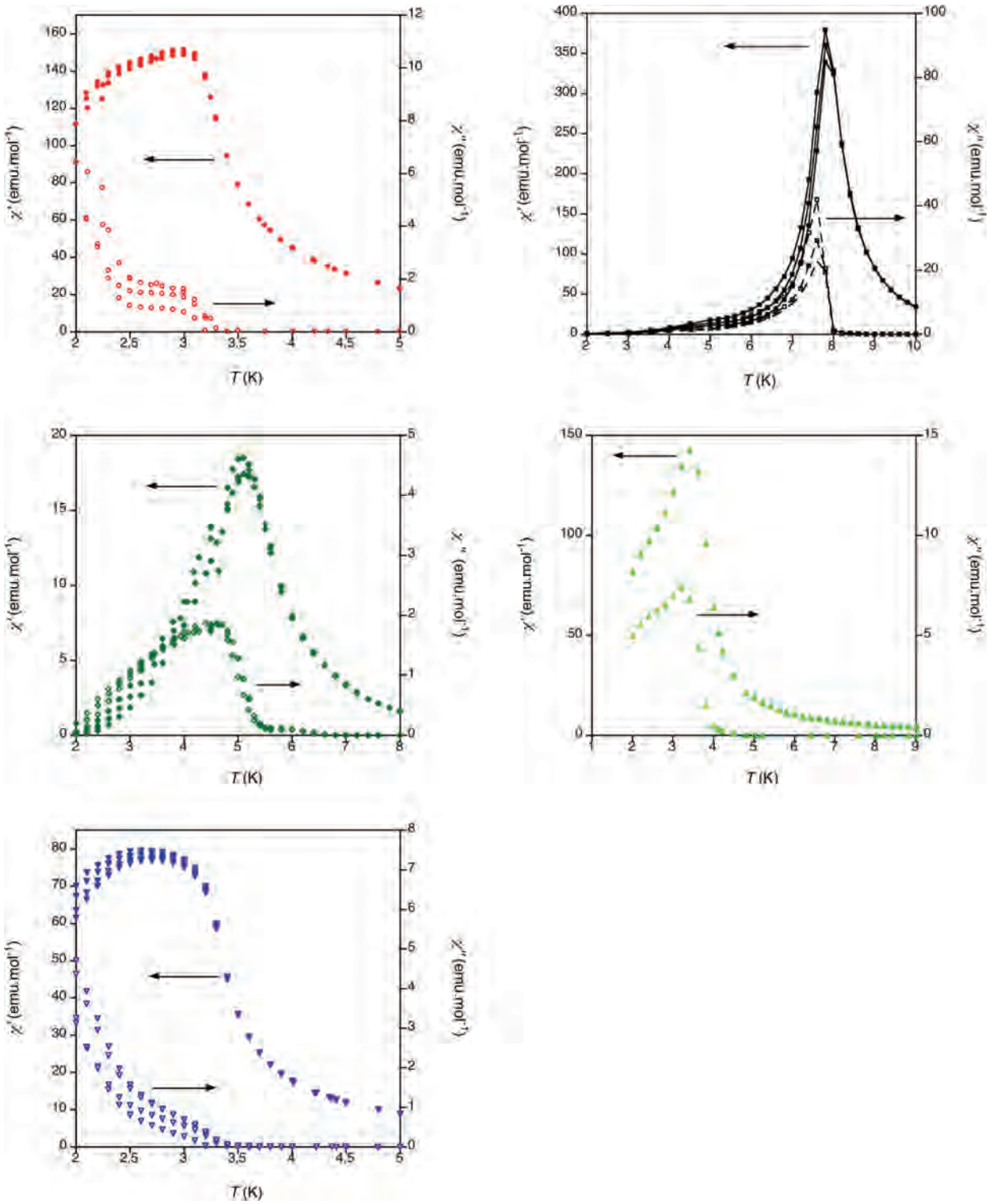

Figure 7. ac susceptibility measurements between 1−1000 Hz for **1**−**5**. Solid symbols represent in-phase signals and open symbols the out-of-phase one. M^{II} = Mn (•), Fe (▼), Co (○), Ni (▲), and Cu (▼).

This fact forces some of the oxalate molecules to act as terminal ligands, thus resulting in the existence of two different types of M^{II} and M^{III} metallic centers. Therefore, M^{II} centers can be divided into $M^{II}1$ and $M^{II}2$ ions in a 2:1 ratio. Whereas $M^{II}1$ ions are surrounded by two chelating oxalate bridging ligands and two coordinating water molecules in an octahedral geometry, the $M^{II}2$ centers are only coordinated to chelating oxalate ligands. Consequently two different $[M^{III}(ox)_3]^{3-}$ unities can be also observed in the same ratio, whereas one of them is binded to three bis-chelating oxalate bridging ligands that connects it to three M^{II} ions the other is coordinated to one oxalate molecule, which acts as a terminal ligand and thus it is directly connected to only two M^{II} ions. Terminal oxalate ligands are connected to M^{II} ions through hydrogen bonding interaction with the coordinating water molecules, in consequence the metal to metal distance increases from the 5.43−5.45 Å range, typical

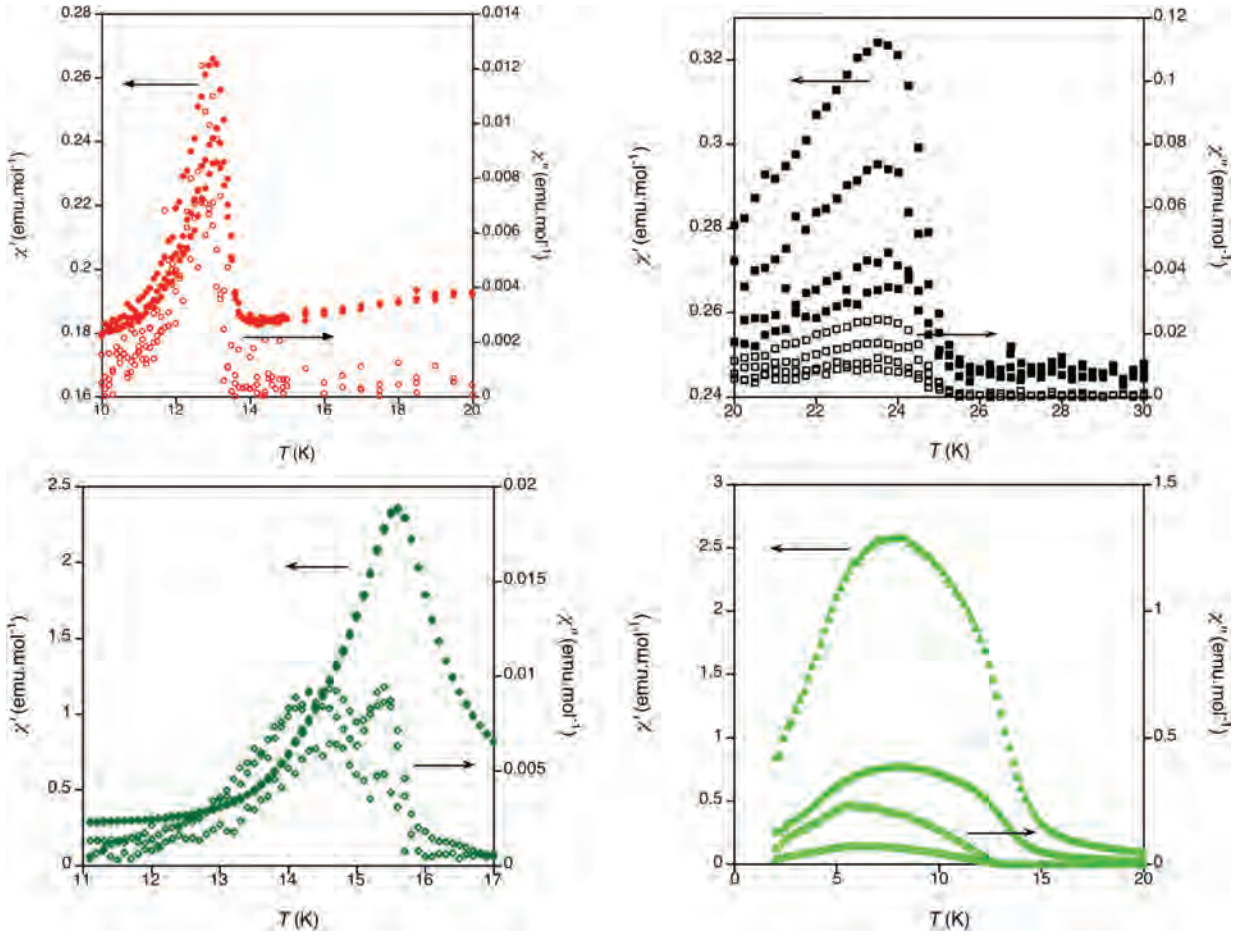

Figure 8. ac susceptibility measurements for **6**−**9**. Solid symbols represent in-phase signals and open symbols the out-of-phase one. M^{II} = Mn (•),Fe (▼), Co (◦), and Ni (▲).

Table 3. Magnetic Parameters for the Series $[K(18\text{-crown-6})]_3[M^{II}_3(H_2O)_4\{M^{III}(ox)_3\}_3]$ (M^{III} = Cr, Fe; M^{II} = Mn, Fe, Ni, Co, Cu; ox = $C_2O_4^{2-}$) [a]

$M^{III}M^{II}$	C [emu K mol^{-1}]	θ [K]	T_c [K]	M_S [μ_B]	M_R [μ_B]	H_{Coer} [kG]
CrMn	16.39	2.23	3.5	23.90	<0.01	
CrFe	14.08	11.17	8	15.55	2.32	0.13
CrCo	16.13	2.21	6	13.66	3.69	0.17
CrNi	9.27	21.91	4.5	14.63	4.50	0.79
CrCu	6.66	9.61	3.2	11.58	<0.01	
FeMn	26.72	−71.32	14	2.01	1.14	0.18
FeFe	24.30	−80.02	25.5	1.93	<0.01	
FeCo	20.29	−49.68	16	2.13	0.95	15.3
FeNi	17.64	−64.77	11.5	6.64	<0.01	0.23

[a] Curie constant (C), Weiss constant (Θ), critical temperature (T_c), saturation magnetization (M_S), remnant magnetization at 2 K (M_R), and coercive field at 2 K (H_{Coer}). $S_{CrIII} = 3/2$, $S_{FeIII} = 5/2$, $S_{MnII} = 5/2$, $S_{FeII} = 3/2$, $S_{CoII} = 2$, $S_{NiII} = 1$, $S_{CuII} = 1/2$.

for a bis-chelating oxalate bridge to 7.77 Å. Within the anionic polymer all of the M^{III} ions are homochiral and have opposite chirality to that of the M^{II} metallic centers. If the hydrogen bonding is taken into account, the oxalate-bridged layer can be considered as a precursor of the well-known 2D hexagonal network (Figure 2). Indeed, if the coordinated water molecules were eliminated and the corresponding hydrogen-bonded oxalate ligands were taking its place as chelating moieties, the result would be the formation of the typical honeycomb structure.

Cationic layers are formed by pseudohexagonal packing of $[K(18\text{-crown-6})]^+$ complexes. The crown ether molecules' mean plane is oriented essentially perpendicular to the c axis, forming an angle of approximately 26° with the ab plane. This specific orientation is probably determined by the presence of electrostatic interactions (d_{K1-O11} = 3.179(8) Å and d_{K1-O12} = 3.103(9) Å) along with hydrogen bonding ($d_{O20-O37}$ = 2.738(1)) between the extended anionic network and the cationic complexes (Figure 3). The interlayer separation of 8.18 Å, defined as the distance between the mean planes of adjacent anionic layers, is in the same range than those reported for previous oxalate-based 2D phases. The location of the cationic crown ether complexes with respect to the anionic 2D layers represents an interesting structural feature for this sort of compounds. They appear slightly displaced from the central position of the pseudohexagonal channels defined by the packing of the oxalate-based framework along the c axis. This point contrasts with that observed in the $[M^{II}Cp^*_2][M^{II}M^{III}(ox)_3]$ family, where the organometallic cations exhibit a staggered conformation and are located in the central position of the hexagonal channels. This distinctive feature along with the network fragmentation might be explained by two main reasons:

1) The larger diameter of the $[K\text{-}(18\text{-crown-6})]^+$ complex with respect to the $[M^{II}Cp^*_2]^+$ organometallic cation, which promotes the network fragmentation as a consequence of the bigger volume of the moiety to be located in the interlayer space. In fact, the complexes size was estimated from the length of the symmetry axis perpendicular to the main one

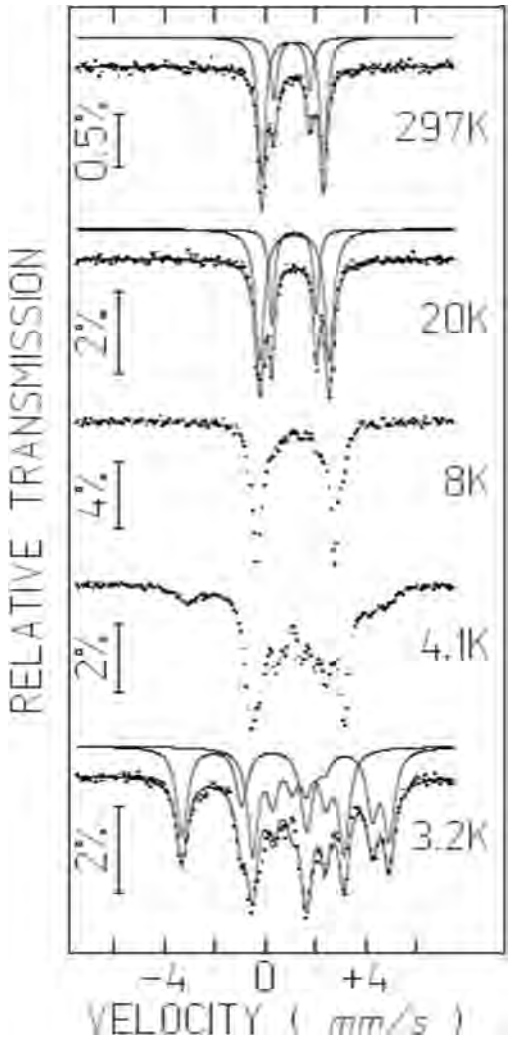

Figure 9. Mössbauer spectra of $[K(18\text{-crown-}6)]_3$ $[Fe_3(H_2O)_4\{Cr(ox)_3\}_3]$ taken at different temperatures. The lines over the experimental points are the sum of the contributions of iron(II) in different crystallographic sites, shown slightly shifted for clarity.

(Supporting Information).

2) The presence of electrostatic and hydrogen bonding interactions between the terminal oxalate groups in the fragmented anionic 2D network and the cationic complex, which forces the $[K\text{-}(18\text{-crown-}6)]^+$ units to be displaced from the center of the pseudohexagonal channels toward the oxalate framework.

Magnetic Properties. $M^{II}Cr^{III}$: magnetic susceptibility measurements for **1**−**5** derivatives present a constant $\chi_M T$ product value as the temperature decreases down to 15 K (Figure 4). The $\chi_M T$ product in the high-temperature regime (150−300 K) can be fitted to a Curie−Weiss law, giving Curie constant values in good agreement with the expected spin-only values except for the cobalt(II) derivative. In the $Co^{II}Cr^{III}$ compound, this deviation was expected attending to the high local anisotropy for octahedral cobalt(II), induced by the existence of a first-order orbital contribution to the magnetic momentum. Indeed, all of the compounds present a positive θ value in the paramagnetic regime, suggesting the presence of ferromagnetic interactions, as expected between chromium(III) and neighboring divalent ions through a bis-bidentate chelating oxalate linker. Below 15 K, magnetization abruptly increases, reaching a maximum in the $\chi_M T$ product that corresponds to a steep jump in the χ_M versus T plot, suggesting the existence of long-range magnetism in these systems. After this jump, magnetization values tend to saturation for all of the compounds, reaching a ferromagnetic ordered state.

To confirm the existence of magnetic ordering and define more precisely the critical ordering temperatures, ac magnetic measurements were performed (Figure 7). All of the compounds present a maximum in both the in-phase signal (χ'_M) and the out-of-phase signal (χ''_M). We have considered the critical temperature (T_c) for these systems as the higher-temperature nonzero out-of-phase signal. In the manganese(II) (**1**) and copper(II) (**5**) derivatives, the χ''_M signal presents two contributions, the first of them corresponds to the reach of an ordered magnetic state above 2.5 K, whereas the second one, which shows slightly frequency dependence, might be associated to domain-wall movements in the ferromagnetic ordered state, as previously reported in several low-dimensional molecule-based magnets.[31,32] **2**, **3**, and **4** present a sharp nonfrequency-dependent peak in both the in- and out-of-phase signals in a 4.5−8 K threshold. Field dependence of the magnetization at 2 K confirms the ferromagnetic nature of the magnetic ordering in these systems (Figure 6). Indeed, a rapid saturation of the magnetization is observed, with M_S values in good agreement with parallel alignment of interacting spins ($S_{CrIII} = {}^3/_2$, $S_{MnII} = {}^5/_2$, $S_{CoII} = {}^3/_2$, $S_{FeII} = 2$, $S_{NiII} = 1$, and $S_{CuII} = {}^1/_2$). However, the magnetic field required to reach saturation is rather large, and therefore the observed saturation magnetization values are slightly smaller than expected as previously reported for the $[NR_4]^+$ derivatives.[2] This fact can be attributed to the presence of spin canting in the ferromagnetic ordered states. All of the compounds present hysteresis loops at 2 K (Supporting Information) and can be classified as soft magnets, being the largest coercive field 790 G for the nickel(II) derivative (Table 3).

$M^{II}Fe^{III}$: magnetic susceptibility measurements for the (**6**−**9**) derivatives were performed (Figure 5). All of the compounds present a clear decrease in the $\chi_M T$ product values as the temperature decreases. The high-temperature regime (150−300 K) has been fitted to a Curie−Weiss law, giving Curie constant values (C) in good agreement with expected spin-only values. The large negative values of the Weiss constants are indicative of the presence of antiferromagnetic interactions between neighboring metallic centers in all the cases as expected for the superexchange between iron(III) and divalent metallic ions when the oxalate ligand acts in a bis-bidentate chelating fashion. Below 25 K, the $\chi_M T$ product presents an increase in the magnetization reaching a maximum that corresponds to an abrupt jump in the χ_M versus T plot, suggesting the onset of long-range magnetic ordering in these systems.

(40) Coronado, E.; Galan-Mascaros, J. R.; Gomez-Garcia, C. J.; Martinez-Ferrero, E.; Almeida, M.; Waerenborgh, J. C. *Eur. J. Inorg. Chem.* **2005**, 2064–2070.
(41) Iijima, S.; Koner, S.; Mizutani, F. *J. Radio. Nucl. Chem.* **1999**, *239*, 245–249.

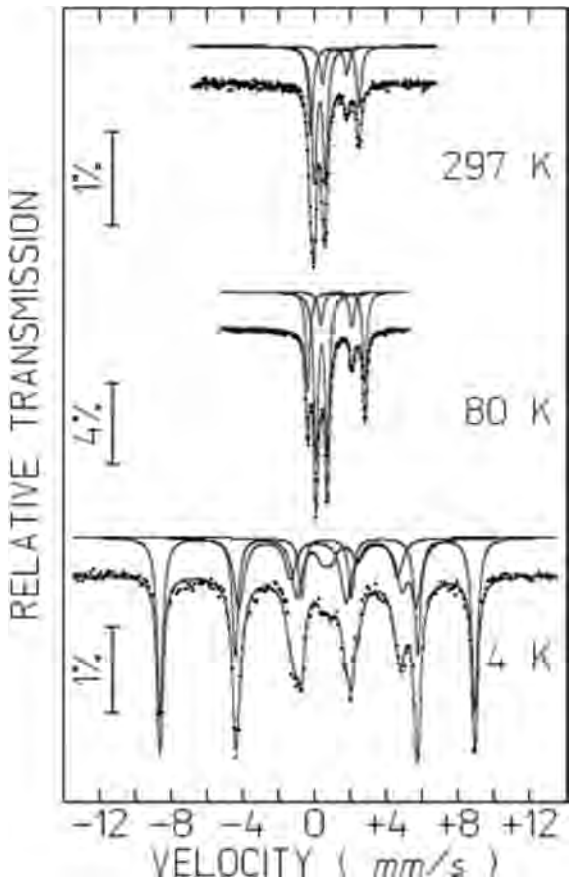

Figure 10. Mössbauer spectra of $[K(18\text{-crown-}6)]_3\,[Fe_3(H_2O)_4\{Fe(ox)_3\}_3]$ taken at different temperatures. The lines over the experimental points are the sum of the contributions of iron(III) and iron(II) in different crystallographic sites, shown slightly shifted for clarity.

Table 4. Crystallographic Data for Compound $[K(18\text{-crown-}6)]_3[Mn_3(H_2O)_4\{Cr(ox)_3\}_3]$ Extracted from [30]

formula	$H_{80}C_{54}Cr_3Mn_3K_3O_{58}$
size [mm]	0.3 × 0.3 × 0.2
fw	2095.30
T [K]	293(2)
λ [Å]	0.71073
cryst syst	monoclinic
space group	$C2/m$
a [Å]	26.7760(6)
b [Å]	20.0490(5)
c [Å]	18.1900(5)
α [°]	90
γ [°]	115.9321(9)
β [°]	90
V [Å^3]	8781.8(4)
Z	4
ρ_{calcd} [g cm^{-3}]	1.585
$\mu(Mo_{K\alpha})$ [cm^{-1}]	1.025
$F(000)$	4288
2Θ limit	2.59−26
GOF	0.895
$R_1{}^a$	0.0538
$R_2{}^b$	0.1513

^{a} $R_1 = \Sigma(F_0 - F_c)/\Sigma(F_0)$. ^{b} $R_2 = [\Sigma[\omega(F_0^2 - F_c^2)^2]/\Sigma[\omega(F_0^2)^2]]^{1/2}$; $\omega = 1/[\sigma^2(F_0^2) + (0.0343P)^2 + 2.4502P]$; $P = (F_0^2 + 2F_c^2)/3$.

Ac measurements performed on these compounds exhibited critical temperatures from 11.5, for the $Ni^{II}Fe^{III}$ case, up to 25.5 K for the $Fe^{II}Fe^{III}$ system (Figure 8). Manganese(II) and iron(II) derivatives exhibit a sharp, well-defined nonfrequency-dependendent in-phase (χ'_M) peak, whereas this signal gets broader for the nickel(II) and cobalt(II) cases. In particular, the iron(II) derivative in-phase maximum intensity shows frequency-dependent variations. Concerning the out-of-phase signal (χ''_M), except for the sharp nonfrequency dependent peak observed in the manganese(II) case, all of the compounds exhibit broad maxima whose intensity shows tiny frequency dependence. In particular, for the cobalt(II) compound, apart from the sharp maximum at 15.4 K, which must be connected to the onset of long-range magnetic ordering, a frequency-dependent singularity can be observed.

To confirm the nature of the magnetic ordering field dependence of the magnetization at 2 K was studied (Figure 6). All of the compounds, apart from the nickel(II) derivative, present a linear increase of the magnetization with the applied field, reaching small magnetization values at 5 T. Taking into account that saturation is still far from the perfect ferromagnetic state, the rapid increase of the magnetization with the applied field (up to 3.5 μ_B) observed for the nickel(II) derivative might be induced by the softness of the nickel(II) ion in an octahedral environment. Except for the manganese(II) derivative, where as the two interacting spins are equal ($S_{FeIII} = S_{MnII} = {}^5/_2$) and magnetic ordering must arise from the existence of spin canting in the ordered antiferromagnetic state, the rest of compounds present ferrimagnetic ordering due to the antiferromagnetic interaction between non-equivalent spins ($S_{FeIII} = {}^5/_2$, $S_{CoII} = {}^3/_2$, $S_{FeII} = 2$, $S_{NiII} = 1$). Hysteresis loops at 2 K were observed for all of the compounds (Supporting Information). Remarkable attention must be payed to the cobalt(II) derivative presenting the highest coercive field (1530 G) if compared to the rest of the compounds that behave as soft ferrimagnets. This fact must be somehow related to the larger anisotropy of octahedral cobalt(II) ions that introduces larger hardness to the resulting magnetic material.

Compared to the classical $[XR_4][M^{II}M^{III}(ox)_3]$ 2D honeycomb networks, whose critical temperatures range from 6 to 12 K for the chromium(III) derivatives and from 28 to 45 K for the iron(III) analogues, magnetic ordering arise at lower temperatures in the studied compounds. Fragmentation of the magnetic framework might be the responsible for this fact. Indeed, in this case two-thirds of the oxalate bridges have been substituted with hydrogen bonding, thus resulting in an elongation of the intermetallic distances and weaker magnetic superexchange through the $M^{II}-H_2O-ox-M^{III}$ bridge.

Mössbauer spectroscopy.[57] Fe Mössbauer spectroscopy is a very sensitive and accurate tool for gathering information about the magnetic, electronic, time-dependent, and dynamical properties of iron-containing molecule-based magnets. Indeed, remarkable information concerning the magnetic structure in the $[NBu_4]^+$ bidimensional oxalate-based magnets derivatives was previously obtained by means of this technique.[33–35] Mössbauer spectra of **2** above 20 K show 4

(42) Ono, K.; Ito, A. *J. Phys. Soc. Jpn.* **1964**, *19*, 899.
(43) Coronado, E.; Galan-Mascaros, J. R.; Marti-Gastaldo, C.; Ribera, A. *Chem. Mater.* **2006**, *18*, 6112–6114.
(44) Baylar, E. M., J. M. J. *Inorganic Syntheses*; New York: McGraw-Hill Book Co., 1939; p v.

peaks (Figure 7), which may be fitted by two quadrupole doublets. The estimated isomer shift (*IS*) and quadrupole splittings (*QS*) are typical of high-spin iron(II), $S = 2$ (Supporting Information). Within experimental error the estimated relative areas are very close to the 2:1 ratio expected from crystal structure data, the site with the largest *QS* corresponding to iron(II) coordinated by two oxalate ligands and two water molecules, namely site M1. The site presenting a lower *QS* value is therefore attributed to iron(II) coordinated by three oxalate ligands, hence site M2.

At 10 K, the peak widths of the inner doublet, M2, have increased significantly, and at 8 K this contribution may no longer be described by a quadrupole doublet (Figure 7). This fact suggests a drastic decrease in the dynamics of iron magnetic moments, μ_{Fe}, on the M2 sites as the temperature decreases. This slowing down of the changes in μ_{Fe} directions is not yet observed for the M1 sites at 8 K. In fact, the outer doublet, M1, is still observed down to 4.1 K, although at this temperature a significant fraction of the M1 contribution already evidences slow relaxation of the μ_{Fe} directions, typical of magnetic ordering. Apparently, the transition observed in magnetization data corresponds to a gradual freezing of the μ_{Fe} directions as the temperature decreases below 8 K, occurring first for the M2 sites.

At 3.2 K, all of the μ_{Fe} directions, both on M1 and M2 sites, seem to be frozen as there is no sign of quadrupole doublets. The spectrum shape however clearly indicates that the contributions to the spectra may not be described by simple magnetic sextets. This implies that the quadrupole hyperfine interactions cannot be treated as a perturbation of the magnetic hyperfine interactions. The position and relative intensities of the absorption lines for the magnetically ordered iron(II) on both the M1 and M2 sites were therefore calculated by solving the complete Hamiltonians for the hyperfine interactions in both the excited and ground nuclear states of the ^{57}Fe nuclei, following the procedure described by Ruebenbauer and Birchall.[36]

The best fit of the spectrum was obtained assuming that for iron(II) on both the M1 and M2 sites the angles between the magnetic hyperfine field, B_{hf}, and the main axis of the electric field gradient, V_{zz}, is $\theta = 90°$ and between B_{hf} and V_{xx} is $= 0°$. The remaining estimated parameters are summarized in the Supporting Information.

The Mössbauer spectra of **7** at room temperature and 80 K show two doublets similar to those found for **2** (Figure 8). Their parameters are also consistent with high-spin iron(II). As expected, an additional doublet with parameters typical of high-spin iron(III) is also observed. The relative areas of these three contributions are consistent with crystallographic data. As in the case of **2**, iron(II) on M1 sites has the largest *QS*. Contributions from iron(III) on different crystallographic sites are not resolved.

At 4 K, in agreement with magnetization data, all the μ_{Fe} directions are frozen. A sextet with large B_{hf}, typical of high-spin $S = {}^5/_2$ iron(III) is clearly visible. The presence of the iron(II) contributions is clearly revealed by the resolved absorption peak at approximately 5 mm/s and the large intensities of the absorption peaks at approximately −4 mm/s and +6 mm/s. In fact, the observed absorption intensities at −4 mm/s and +6 mm/s may not be explained by the iron(III) sextet alone. These latter peaks are the result of the overlap of iron(II) peaks with peaks 2 and 5 of the iron(III) sextet. Two contributions from the magnetically ordered iron(II) were therefore fitted as in the case of **2**. Parameters leading to the best fit are summarized in the Supporting Information.

For both compounds, B_{hf} and therefore μ_{Fe} of iron(II) are perpendicular to the main axis of the electric-field gradient as in the case of the oxalate-bridged bimetallic Fe−Fe or Fe−Cr complexes[37–41] or the simple Fe(ox)·2H$_2$O,[42] which form extended bidimensional magnetic networks. If in the title compounds, V_{zz} is perpendicular to the oxalate layers, as in the case of the oxalate-bridged bimetallic Fe−Fe or Fe−Cr complexes crystallizing in rhombohedral or hexagonal space groups, then μ_{Fe} of iron(II) should be parallel to the oxalate layers. It should also be noted that the magnitude of the B_{hf} of iron(II) on the M1 sites in **2** and **7** compounds is as far as we know the largest reported for iron(II) in the oxalate-bridged bimetallic Fe−Fe or Fe−Cr complexes or even in Fe(ox)·2H$_2$O.

Conclusion

In this article, we have presented the synthesis and magnetic characterization for the 2D oxalate-based magnets with general formula: [K(18-crown-6)]$_3$[M$^{II}_3$(H$_2$O)$_4${M^{III}(ox)$_3$}$_3$] (M^{III} = Cr, Fe; M^{II} = Mn, Fe, Ni, Co, Cu; ox = $C_2O_4^{2-}$). All of the isolated compounds are isostructural and present long-range magnetic order at low temperatures. Whereas the Cr^{III}M^{II} derivatives behave as ferromagnets with critical temperatures up to 8 K, the Fe^{III}M^{II} series present ferri- or weak ferromagnetic ordering up to 26 K. These magnetic layered systems structurally remind us of the well-known 2D honeycomb networks previously reported by Okawa et al. in the early 90s[2,5] but present slight differences. In this particular case, the bulky planar [K-(18-crown-6)]$^+$ cationic complex does not penetrate in the polymeric anionic network, whereas the [NBu$_4$]$^+$ derivatives present one fraction of the butyl organic fragments inserted into the hexagonal holes defined by the anionic network. This point suggests that the templating effect usually attributed to the cation in the assembling and isolation of this sort of compounds is not necessary for the formation of this particular polymeric bimetallic oxalate network. The fragmentation of the 2D anionic framework connectivity appears as another important difference. This fact might be introduced by the size of the [K-(18-crown-6)]$^+$ and the existence of hydrogen bonding interactions between the crown ether and the water molecules coordinated to one

(45) *Collect*, Vol. Nonius BV; 1997−2000.

(46) Otwinowsky, Z.; Minor, W. In *Processing of X-ray Diffraction Data Collected in Oscillation Mode*; Carter, C. W. Jr., Sweet, R. M., Eds.; Academic Press: New York, 1997; Vol. 276.

(47) Altomare, A.; Burla, M. C.; Camalli, M.; Cascarano, G. L.; Giacovazzo, C.; Guagliardi, A.; Moliterni, A. G. G.; Polidori, G.; Spagna, R. *J. Appl. Crystallogr.* **1999**, *32*, 115–119.

(48) Sheldrick, G. M. *SHELXL-97*; University of Göttingen: Göttingen, Germany, 1997.

(49) *CrystalMaker*; CrystalMaker Software: Oxford, UK, 2006.

(50) *Crystal Diffract*; CrystalMaker Software: Oxford, UK, 2006.

(51) Holland, T. J. B.; Redfern, S. A. T. *Mineral. Mag.* **1997**, *61*, 65–77.

fraction of the M^{II} ions in the polymeric network. For a deeper understanding of the possible relationship between the crown ether molecule size and the fragmentation of the network, we are currently studying the effect introduced by smaller crown ether derivatives in the formation of analogous oxalate-based systems.

We would also like to remark that the solubility of these compounds in water and polar solvents in comparison with the insolubility of the rest of previously reported 2D and 3D oxalate-based frameworks. Although magnetic properties of the original solids are not retained in solution, evaporation of the solvent can easily regenerate original coordination polymers. This point allows for the obtention of large good-quality single crystals and turns these materials into perfect candidates for the preparation of novel hybrid materials by means of intercalation chemistry[43] and materials processing techniques. We are currently investigating the use of this sort of systems in the organization of nanostructured magnetic patterns on surfaces by means of inkjet-printing and nanolithographic techniques.

Acknowledgment. Financial support from the European Union (NoE MAGMANet, MERG-CT-2004-508033), the Spanish Ministerio de Educación y Ciencia (Project Consolider-Ingenio in Molecular Nanoscience, CSD2007-00010, project MAT2004-03849 and project MAT2007-61584), and the Generalitat Valenciana are gratefully acknowledged. C.M.G. thanks the MEC for a predoctoral fellowship. J. M. Martínez-Agudo, for his help with the magnetic measurements, is also gratefully acknowledged.

Supporting Information Available: Bulky space representation of the cationic complexes $[K\text{-}(18\text{-crown-}6)]^+$ and $[FeCp^*_2]^+$, X-ray powder diffraction profiles for **1**−**9** and estimated parameters for iron from the Mössbauer spectra of **2** and **7** obtained at different temperatures, hysteresis cycles for **1**−**9** at 2 K. This material is available free of charge via the Internet at http://pubs.acs.org.

IC800418K

(52) Waerenborgh, J. C.; Figueiredo, M. O.; Cabral, J. M. P.; Pereira, L. C. J. *J. Solid State Chem.* **1994**, *111*, 300–309.